A high-resolution spectroscopy study on bidimensional ordered structures: the (1 × 1) and (1 × 2) phases of Bi/InAs(110)

1999 J. Phys.: Condens. Matter 11 7447

(http://iopscience.iop.org/0953-8984/11/39/303)

J. Phys.: Condens. Matter **11** (1999) 7447–7461. Printed in the UK PII: S0953-8984(99)03733-9

A high-resolution spectroscopy study on bidimensional ordered structures: the (1 × 1) and (1 × 2) phases of Bi/InAs(110)

V De Renzi, Maria Grazia Betti, V Corradini, P Fantini, V Martinelli and Carlo Mariani

Istituto Nazionale per la Fisica della Materia, Dipartimento di Fisica, Università di Modena e Reggio Emilia, via G Campi 213/A, I-41100 Modena, Italy

E-mail: vderenzi@unimo.it

Received 26 April 1999

Abstract. The room-temperature growth of bismuth on the InAs(110) surface and the Bi-(1 × 1) and Bi-(1 × 2) ordered phases have been studied by means of high-resolution ultraviolet photoemission and high-resolution electron-energy-loss spectroscopy. A modified Stransky–Krastanov growth mode at room temperature and the stability of the (1 × 2)-symmetry phase in the 480–580 K annealing temperature range are deduced by quantitative analysis of the core-level data and Auger spectra. A Bi 5d and In 4d core-level analysis is presented, and discussed according to a recently proposed model for the (1 × 2) overlayer reconstruction. The formation of Bi-derived electronic states has been followed during the growth of the (1 × 1)-symmetry phase, showing a semiconducting behaviour at the monolayer coverage, with a well-defined gap state at 0.39 eV binding energy related to the Bi p-like dangling bonds. The (1 × 2)-Bi phase is metallic, as indicated by the well-defined Fermi edge and by the metallic-like quasi-elastic peak tail in the energy-loss spectra. The metallicity and the electronic structure of the (1 × 2)-Bi phase are discussed in relation to the available geometric structure.

1. Introduction

Adsorption of group V elements on the III–V(110) surfaces has been widely experimentally and theoretically addressed in the last two decades, thanks to their unreactive, non-disruptive, and ordered growth. In particular, surface chemical bonding, electronic structure, growth, and ordering of these systems have been intensively studied, revealing common features as well as differences upon changing both substrate and adsorbate. In the following, we briefly recall some of these features, while we refer the reader to Schmidt *et al* [1] for a comprehensive and exhaustive review on the subject.

Room-temperature (RT) growth of group V semimetals on III–V(110) surfaces is well described by the Stransky–Krastanov (SK) model, in which the completion of the first monolayer is followed by tridimensional (3D) island formation. The RT-prepared monolayer structure displays a (1 × 1)-symmetry epitaxial continued-layer structure (ECLS) [2], with the adatoms continuing the underlying substrate bulk-like structure. Due to the adsorbate isovalency and to the similar bonding geometries, almost all of the (1 × 1)–V/III–V(110) systems present similar semiconducting electronic band structure, in which states related to anion- and cation-bonded adatoms can be distinguished [3, 4]. However, different orbital

0953-8984/99/397447+15$30.00

energies and differences in bond lengths and angles induce some quantitative changes between the electronic structures of Bi and Sb monolayers on III–V(110) surfaces. In particular, Bi-induced states significantly extend into the bulk gap [5–7], while this is not the case for the Sb-induced states [8, 9].

For both Bi and Sb, an appropriate annealing procedure on thick overlayers produces ordered and stable monolayers. While in the case of Sb this procedure always produces a (1×1) structure, for Bi several different superstructures are observed: Bi adsorption on GaAs(110) exhibits regular dislocations along the Bi chains, with missing adatoms every six unit cells [5, 10]. The Bi covalent radius is larger than that of Sb by almost 4%, so the presence of vacancies can be attributed to strain release induced by lattice mismatch between Bi and the substrate. On the other hand, the (1×2) reconstruction observed for the Bi/InAs and Bi/GaSb (110) systems [10] cannot be solely attributable to lattice mismatch, as these substrates present a larger lattice constant than GaAs, and good matching with the Bi covalent radius. Remarkably, at variance with the semiconducting character of the (1×1)-Bi phases [1], all of the observed (1×2)-Bi/III–V(110) layers display metallic character [13–16].

In order to understand the fundamental reason for this surface reconstruction, a characterization of both the electronic and structural properties of these phases is needed. A comparison between 2D-ordered systems which only differ in their geometrical structure (i.e. the (1×1) and (1×2) phases of Bi on InAs(110)) can shed light on the correlation between their geometric, electronic, and dielectric properties. In spite of the great amount of literature on the (1×1) phases of group V atoms on III–V(110) surfaces [1], only little is known about the reconstructed structures. As far as we know, the only determinations of the geometric structure of (1×2)-Bi/III–V(110) phases are a grazing-incidence x-ray diffraction (GIXD) study on the (1×2)-Bi/GaSb(110) system [11] and a very recent GIXD investigation on the (1×2)-Bi/InAs(110) system [12]. According to these experiments, the (1×2)-Bi layer is characterized by a substrate missing-row reconstruction, i.e. with every second zigzag row in the substrate uppermost layer missing along the [001] direction, with Bi atoms forming zigzag chains tilted towards the substrate missing row. Due to this tilting and to the missing-row reconstruction, all atoms in each (1×2)-Bi chain are bonded to the same kind of substrate atom (i.e. anion or cation) of the first and second layer.

In the following we present a comprehensive investigation of bismuth adsorption on the InAs(110) surface, mainly focusing on the evolution of the electronic properties of the interface during RT growth and (1×2) phase formation. After a brief experimental part (section 2), in section 3 results are presented and discussed. In particular, in subsection 3.1.1 we deal with the Bi growth and (1×2)-Bi phase formation, studied by means of core-level photoemission and Auger spectroscopy. We analyse and discuss the In 4d and Bi 5d core levels for the (1×2) phase, along with the available geometrical model for the Bi chain reconstruction. In subsection 3.1.2 the valence band evolution upon Bi adsorption and the electronic properties of the (1×2)-Bi phase are investigated by means of high-resolution ultraviolet photoemission spectroscopy (HRUPS) and high-resolution electron-energy-loss spectroscopy (HREELS). Space-charge layer formation and the band-bending effect are also addressed in subsection 3.2. Finally, in section 4, some concluding remarks are made.

2. Experimental procedure

The experiments were carried out at the LOTUS surface physics laboratory at the Dipartimento di Fisica, Università di Modena e Reggio Emilia. Valence band and core-level photoemission measurements were performed using a He discharge source, with photon energies of 21.218 eV (He I_α) and 40.814 eV (He II_α), respectively, and a grazing incidence angle to ensure

surface sensitivity. The photoemitted electrons were analysed with a hemispherical analyser (SCIENTA SES-200) with instrumental energy resolution of 15 meV at 10 eV pass energy. Spectra were taken around the Γ point of the Brillouin zone with an angular integration of about ±8°. The Fermi level was determined on a deposited gold layer in electric contact with the semiconductor bar. As will be shown in the following sections, the extremely high luminosity of the energy analyser and its high energy resolution allow measurements of very-low-intensity features in the photoemission spectra. The HREELS spectrometer (Leybold–Heraeus ELS-22), together with low-energy electron diffraction (LEED) and auxiliary equipment for sample cleaning and preparation, complete the ultra-high-vacuum (UHV) system. The HREELS measurements were performed in the specular direction, with an incidence angle equal to the collecting angle of 60°, and with primary beam energy (E_p) of 21.4 eV. The full width at half-maximum (FWHM) of the elastic peak was 15 meV for the plasmon–phonon energy region measurements, while it was degraded to about 25 meV for the electron transition loss region, to ensure a good signal-to-noise ratio. Auger spectra were taken using a double-pass cylindrical mirror analyser (CMA) in the first-derivative mode, with $E_p = 3$ keV. Pressure in the preparation chamber was kept below 10^{-10} mbar during sample preparation and Bi deposition, while it was in the low 10^{-10} mbar range in the main measurement chamber.

The n-type doped InAs(110) single crystal ($n \sim 10^{18}$ cm^{-3}) was cleaved in UHV with the single-wedge technique. Bi was evaporated onto the substrate at RT from a resistively heated quartz crucible, at a rate of about 0.7 Å min^{-1}; its deposition was monitored with an oscillatory quartz crystal microbalance. As will be shown below, Bi grows on InAs(110) at RT in a modified Stransky–Krastanov mode; that is, Bi atoms begin to stick on top of the first monolayer before the latter is completed. Therefore, we define one monolayer as the coverage for which the In 4d surface core-level component disappears, i.e. for which the first Bi layer is completed. The development of the stable (1 × 2) superstructure upon annealing of a several-ML-thick Bi layer was monitored by LEED. The annealing procedure consisted of several annealing steps. For each step the sample was maintained at the annealing temperature for 30 min. This phase was found to be stable between 480 K and 580 K, whilst further annealing eliminated the presence of Bi totally, leaving a clean (1 × 1)–InAs(110) surface.

3. Results and discussion

3.1. Core-level characterization of the (1 × 1)-Bi and (1 × 2)-Bi phases

3.1.1. Growth morphology. The deposition of Bi at RT on the InAs(110) surface was monitored by means of Auger and core-level photoemission spectroscopy. No changes in the Auger lineshapes could be detected, indicating that Bi grows unreactively on the substrate, as already observed by McIlroy *et al* [17]. In figure 1(a) the peak-to-peak intensities of the In MNN, As MNN, and Bi NOO Auger lines are reported as functions of Bi deposition time. In figure 1(b) the corresponding intensities of the In 4d and Bi-5d photoemission core-level peaks are shown. The initial linear dependence of all intensity curves, the subsequent change in slope, and the non-vanishing In 4d bulk peak even at 20 ML coverage (not shown here) are consistent with a Stransky–Krastanov growth mode. Nevertheless, the change in slope is quite smooth, suggesting that growth of subsequent Bi layers starts before the completion of the first monolayer (the modified Stransky–Krastanov mode). More insight into the formation of the Bi overlayer can be achieved by analysing the In 4d core-level photoemission data: the In 4d core-level doublets are shown in figure 2 for some selected coverages, along with their best-fit curves. The best fits are obtained by fitting the data with two Voigt-profile doublets separated

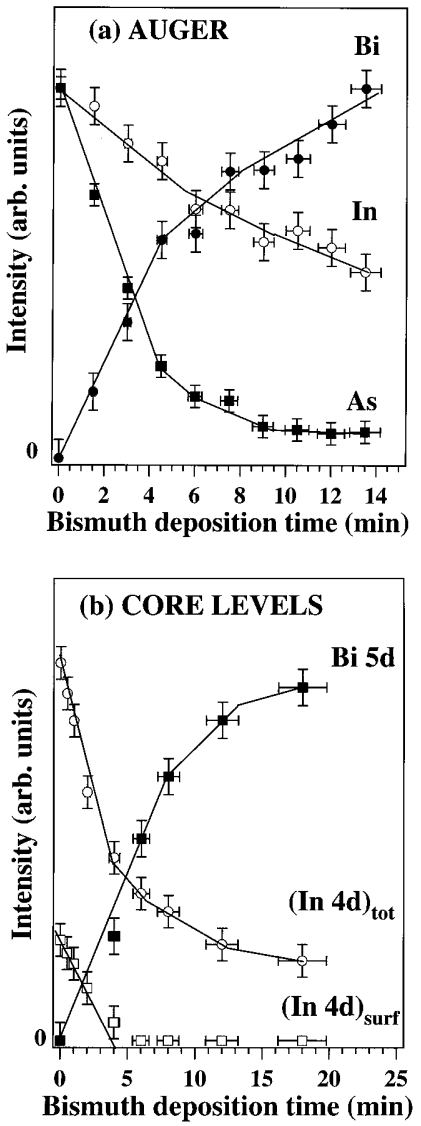

Figure 1. (a) Intensities of the In MNN (empty circles), As MNN (filled squares), and Bi NOO (filled circles) Auger lines as functions of Bi deposition time. (b) In 4d (empty circles) and Bi 5d (filled squares) core-level peak intensities as functions of Bi deposition time. The In 4d surface component intensity is also shown (empty squares). Lines are drawn as guides to the eye.

by 0.27 ± 0.01 eV, related to the bulk and surface components, respectively. In the fitting procedure, the branching ratio, the spin–orbit splitting, the core-hole lifetime (Lorentzian width), and the surface component energy shift (see table 1) were kept constant, and are in agreement with values reported in the literature for the clean surface [18].

The peak intensity, the energy value, and the Gaussian broadening of each doublet were allowed to vary as a function of deposition time. The surface component intensity, reported in figure 1(b), is proportional to the fraction of uncovered InAs(110) surface ($I_s \propto (1-\theta_1)$, where

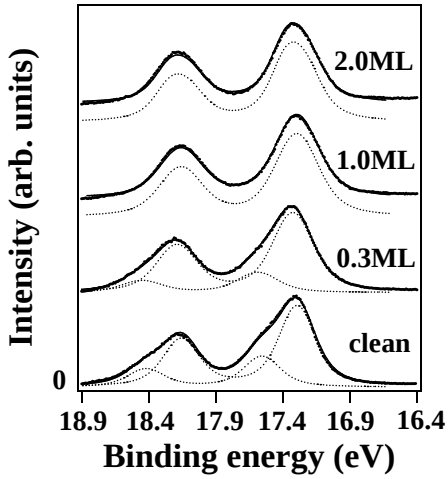

Figure 2. In 4d core-level experimental data (dots) with superimposed best-fit curves (lines), and individual doublet fitting components (dotted lines). Data are taken with photon energy $h\nu = 40.814$ eV. The fitting curves for 1 and 2 ML coverage are vertically shifted for clarity. See the text for details.

Table 1. Fitted parameters of the In 4d core-level peak for different Bi coverages. See the text for details.

Coverage	S–O (eV)	Branching ratio	Γ_{Lor} (eV)	Γ_{Gau} (eV)	$\Delta E_{\mathrm{surf-bulk}}$ (eV)
Clean	0.865	1.7	0.156	0.23	0.27
0.33 ML	0.865	1.7	0.156	0.27	0.27
1.0 ML	0.865	1.7	0.156	0.30	0.27
3.0 ML	0.865	1.7	0.156	0.30	0.27

θ_1 is the coverage of the first Bi layer) and vanishes with the completion of the first epitaxial monolayer. For a perfect SK growth mode, the intensity of the surface component should decrease linearly with coverage, until it vanishes. A deviation from linearity is observed instead in figure 1(b), confirming that the growth of the subsequent layers starts before the completion of the first monolayer†. The analysis of the Bi 5d core levels, shown in figure 3 for the Bi monolayer and multilayer, reveals that three components are already present at about 0.7 ML. The lower- and intermediate-kinetic-energy components are separated by 0.20 ± 0.02 eV and are related to Bi–anion and Bi–cation bonding, while the higher-kinetic-energy one (at 0.18 ± 0.02 eV away from the middle component) can be ascribed to Bi–Bi bonding, as it dominates at high coverage. This attribution of the high-energy component is also supported by a similar peak observed in the Bi 5d level at the Bi/GaAs(110) and Bi/InP(110) interfaces [19] (which present a good SK growth mode) when some clustering starts after completion of the first monolayer. The presence of the high-energy component in the submonolayer coverage stage can be ascribed to some clustering of Bi commencing before the completion of the first monolayer, thus confirming the observed modified SK growth mode.

† It is worth mentioning that the Bi deposition procedure in reference [17] is different from ours, as the sample was annealed to 400 K after each deposition. This may account for the observed differences in the growth mode.

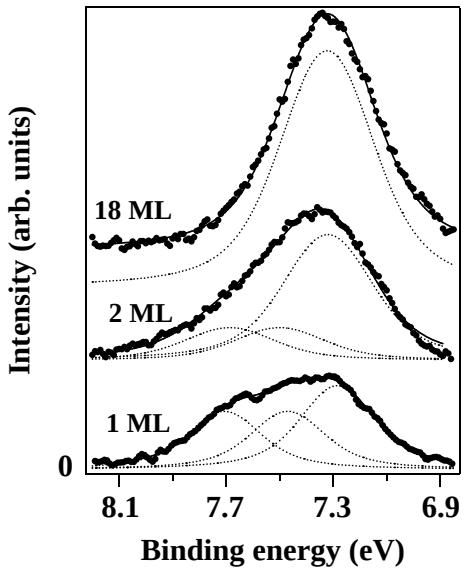

Figure 3. Bi 5d core-level experimental data (dots) with superimposed best-fit curves (lines), and individual fitting components (dotted lines). Data are taken with photon energy $h\nu = 21.218$ eV. The fitting curve for 18 ML coverage is vertically shifted for clarity. See the text for details.

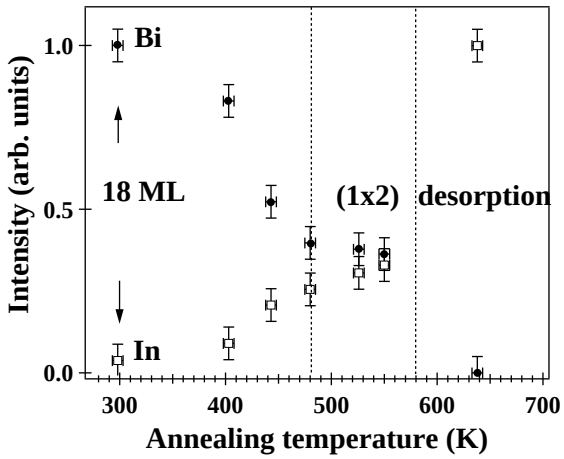

Figure 4. Intensities of the In 4d (empty squares) and Bi 5d (filled circles) core-level peaks as functions of annealing temperature. Peak intensities are normalized to their corresponding maximum values. The Bi initial coverage is 18 ML.

3.1.2. Formation of the (1 × 2)-Bi phase. Upon annealing a several-monolayer-thick Bi layer, a (1 × 2)-symmetry phase is obtained, as checked by LEED. The (1 × 2)-Bi phase starts to appear at around 480 K, becoming more intense and sharp with increasing temperature up to 580 K, beyond which the surface recovers the (1 × 1) symmetry. In figure 4 the intensities of the In 4d and Bi 5d core-level peaks are reported as functions of the annealing temperature. The In peak intensity strongly increases upon annealing to 480 K, while the Bi peak decreases,

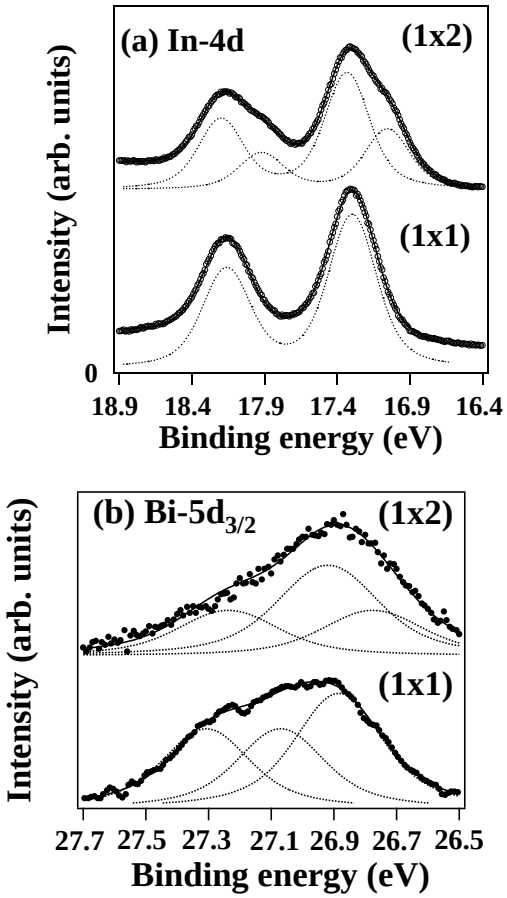

Figure 5. (a) In 4d core levels for the (1 × 1)-Bi phase at 1 ML coverage as deposited and for the (1 × 2)-Bi phase after annealing. Data taken at RT and with photon energy $h\nu = 40.814$ eV. Experimental data (empty circles) and best-fit curves (continuous lines). The individual doublet fitting components (dots) are vertically shifted for clarity. (b) Bi 5d core levels for the (1 × 1)-Bi phase at 1 ML coverage as deposited and for the (1 × 2)-Bi phase after annealing. Data taken at RT and with photon energy $h\nu = 40.814$ eV. Experimental data (filled circles) and best-fit curves (continuous lines). The individual doublet components (dots) are vertically shifted for clarity. See the text for the fitting procedure.

indicating a Bi overlayer rearrangement or a partial Bi desorption. In the stability range of the (1 × 2)-Bi phase both the Bi and In core-level intensities remain almost stable, and correspond to a Bi coverage of approximately 1 ML†. The small intensity variation in this range can be attributed to reordering processes during the (1×2)-Bi phase formation. With further annealing beyond 580 K, the Bi peak disappears, while the In 4d level almost recovers the clean-surface intensity, indicating complete Bi disappearance from the surface. The In 4d core-level peaks do not change their lineshape upon annealing up to about 480 K. They can be well fitted by a single bulk-like doublet, until the (1 × 2)-Bi phase is formed above that temperature. In

† As the surface structure for the (1 × 1)-Bi and the (1 × 2)-Bi phases are quite different, the evaluation of Bi coverage from the core-level intensities is only indicative.

this structural phase a new component appears at 0.280 eV higher kinetic energy, as shown in figure 5(a). The Bi 5d core levels in the (1×2) phase also present a multiple component (figure 5(b)) that could be fitted by either two or three peaks. Despite this arbitrariness, we show a three-component plot, as it fits the data with a more reasonable Gaussian width than the two-component case.

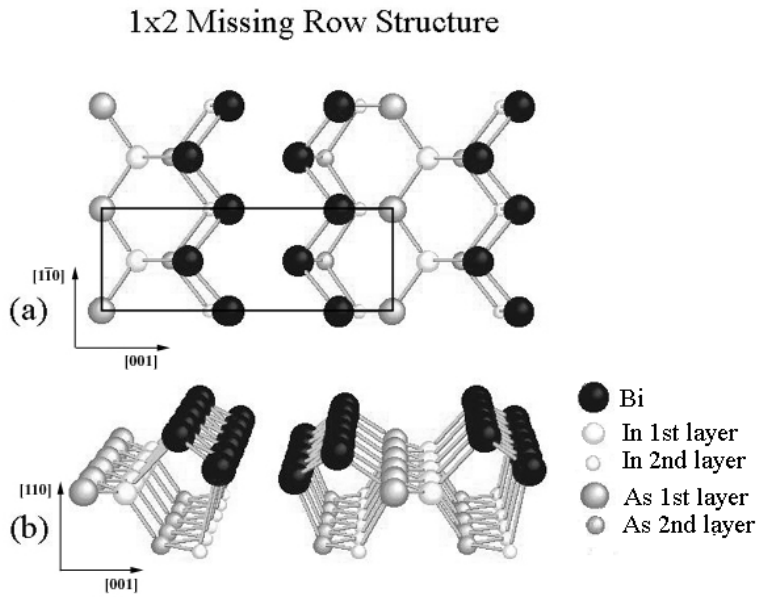

Figure 6. Top (a) and side perspective (b) views of the (1×2)-Bi missing-row structure on InAs(110), as determined by the GIXD experiment and analysis [12].

In order to elucidate the origin of the high-energy component of the In 4d doublet, we collected the In 4d photoelectrons at higher photon energy, using the He II_β satellite photon ($h\nu = 48.372$ eV), thus gaining a higher surface sensitivity. The intensity of the In 4d higher-kinetic-energy component is enhanced (not shown here) with increasing surface sensitivity: this fact demonstrates that this peak originates from the topmost layer In atoms. It also disappears upon recovery of the clean InAs(110) surface, so it cannot be attributed to segregation and clustering of metallic In atoms on the surface [20], as these would remain on the surface after annealing. These core-level data give support to a recently solved complex substrate missing-row reconstruction model [12]. In particular, the absence of the InAs In 4d clean-surface component indicates that all surface dangling bonds are saturated, and therefore rules out a *simple* ECLS-like Bi missing-row structure in the (1×2) phase. The recently solved geometrical model for the (1×2) reconstruction, as derived by GIXD analysis [12], is reported in figure 6. The topmost layer consists of couples of inequivalent one-dimensional (1D) Bi zigzag chains along the [1$\bar{1}$0] azimuthal direction, alternately bonded to In and As atoms. The Bi chains are strongly buckled and their formation causes a major substrate rearrangement, with the appearance of alternate missing rows along the [001] direction. This new structure, accompanied by a charge-transfer rearrangement, might explain the new high-kinetic-energy component in the In 4d core level. However, we cannot exclude the concurrence of final-state

effects: due to the metallic character of the surface, the core hole in the first-layer In atoms could be more efficiently screened than those in the bulk, giving rise to the higher-kinetic-energy component. As regards the Bi 5d core levels, the intensity ratio between the three components suggests that they can be attributed to non-equivalency of three of the four Bi atoms inside each unit cell.

3.2. Electronic properties of the (1 × 1)-Bi and (1 × 2)-Bi phases

The valence band (VB) spectra of the Bi/InAs(110) system as a function of Bi coverage are shown in figure 7 in a perspective view, to enhance the VB shape evolution. The clean-surface valence band presents several features, in particular two main surface structures and the first internal gap. After the first deposition steps, the InAs clean-surface states are quenched, and a general state redistribution takes place. Upon approaching the first monolayer, the electronic states of the (1×1)-Bi monolayer emerge, in particular an occupied state at 16.91 eV kinetic energy (KE) (0.39 eV binding energy, BE), and features in the 13–15 KE range. The interface is semiconducting at 1 ML coverage, whilst the surface gap is gradually closed upon further Bi deposition (3 ML), and the data eventually develop in the Bi bulk-like valence band.

The valence band spectra of a thick Bi layer (18 ML) annealed to progressively increasing

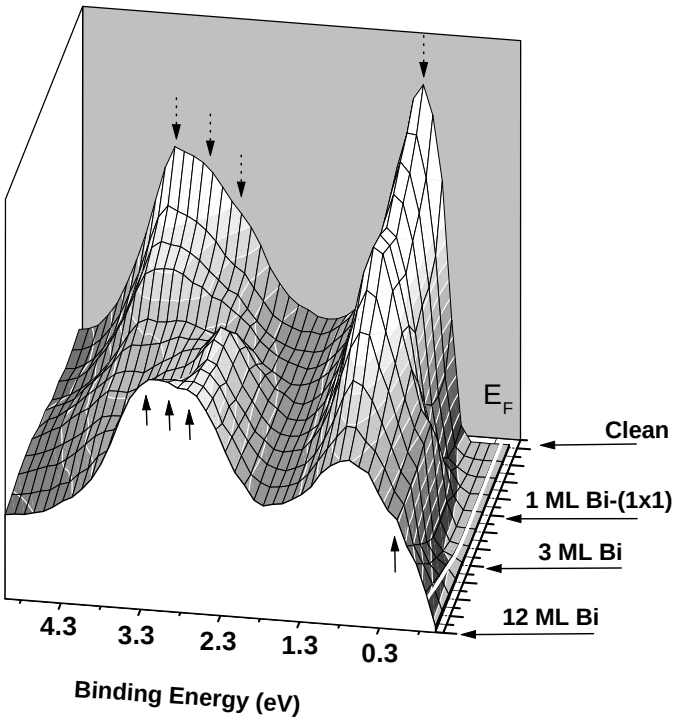

Figure 7. A perspective view of the valence band evolution of the Bi/InAs(110) interface for increasing Bi coverage, taken with photon energy $h\nu = 21.218$ eV. Successive spectra for progressive Bi deposition are stacked along one of the horizontal axes, while the other horizontal axis indicates the photoelectron binding energy. Intensity is displayed on the vertical axes. Dotted and solid arrows indicate clean-surface and Bi-related electronic states, respectively. The Fermi energy position is also indicated.

temperatures are shown in figure 8, in a perspective fashion. Starting from the Bi bulk-like shape, the valence band evolves and becomes much more structured for annealing at about 520 K. All of the spectra between 520 and 580 K are almost identical, demonstrating the stability of the ordered (1×2) structure in this annealing temperature range. The (1×2) phase is metallic, as a finite spectral density is measured at the Fermi level, marking a definite difference from the semiconducting (1×1) phase. Further annealing ensures recovery of the InAs(110) clean-surface valence band, with a clear gap opening. We notice that after annealing at about 480 K the valence band still resembles the thick Bi layer, although the LEED pattern already shows a (1×2) reconstruction. This can be explained by supposing that 3D Bi islands survive on the surface together with patches of the (1×2) structure.

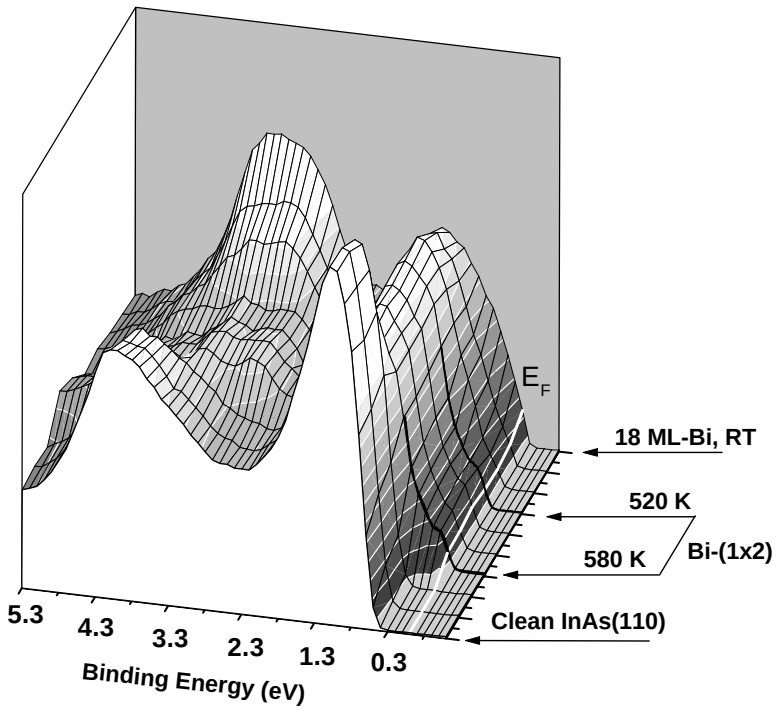

Figure 8. A perspective view of the valence band evolution of the Bi/InAs(110) interface as a function of annealing temperature, taken with photon energy $h\nu = 21.218$ eV. Successive spectra for progressive annealing steps (from RT to 630 K) are stacked along one of the horizontal axes, while the other horizontal axis indicates the photoelectron binding energy. Intensity is displayed on the vertical axes. The Fermi energy position is also indicated. Notice the VB evolution from the bulk-like Bi shape to the semimetallic stable (1×2)-Bi phase, and eventual recovery of the InAs clean-surface gap after complete Bi desorption.

In order to assign the different valence band electronic states and discuss the main features, we present the spectra of the clean (a), (1×1) (b), and (1×2) (c) Bi phases in figure 9. The InAs(110) clean-surface states can be identified as anion-derived (A_i) and cation-derived (C_i), according to the literature [3]. Referring to the pseudopotential calculation performed by Umerski and Srivastava [4] for the (1×1)-symmetry Bi/InAs(110) interface, we can label these states and gain more insight into their character. Our data are in general agreement with previous angle-resolved photoemission results [17]; nevertheless a direct comparison is difficult, due to the different sampling of the surface Brillouin zone (SBZ). The $\sim$16.9 eV KE

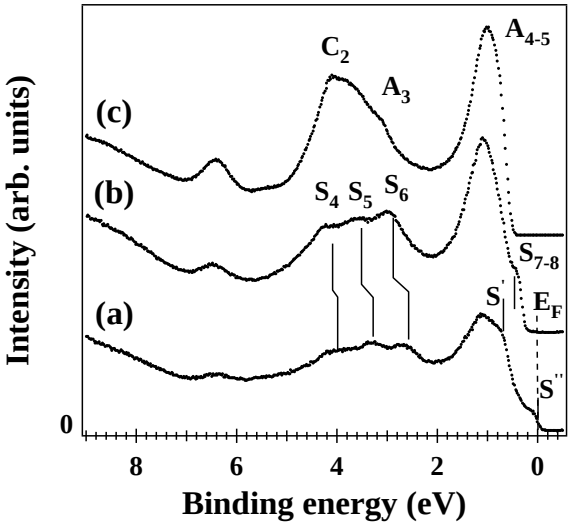

Figure 9. Valence bands of the clean InAs(110) (a), (1 × 1)-Bi (b), and (1 × 2)-Bi (c) phases, taken with photon energy $h\nu = 21.218$ eV. The clean-surface states (A_i and C_i) and Bi-induced states (S_i, S', S'') are indicated (see the text for details). Curves are shifted vertically for clarity. The Fermi energy position is marked by a dashed line.

(∼0.4 eV BE) state characterizing the top of the valence band in the (1 × 1) structure can be attributed to the two highest almost degenerate occupied S_7- and S_8-states, which are mainly derived from the Bi p_z dangling bonds [4]. A similar interpretation has also been given for the analogous state in the 1 ML Sb/InAs(110) system [3]. Along with $S_{7,8}$, other peaks become clearly defined in the 13–15 eV KE region. They can be attributed to S_5 and S_6, related to p-like bonding between the first substrate anion atom and the Bi overlayer. Moreover, from the evolution of the surface states upon Bi adsorption we can infer that the clean-surface state A_3 (14.2 eV KE) evolves into S_5 and S_6 (13.72 eV and 14.32 eV KE, respectively). The C_2-state (13.22 eV KE) of the clean surface probably evolves into the S_4-state (13.1 eV KE), related to the bonding between Bi and substrate cation atoms.

The feature related to the $S_{7,8}$-states in the (1 × 1)-Bi phase is reduced to a faint shoulder in the (1 × 2)-Bi system, while two new structures (labelled as S' and S'') appear at 16.62 eV KE (0.68 eV BE) and 17.16 eV KE (0.14 eV BE). The latter crosses the Fermi energy, causing the surface to be metallic. At higher binding energies, changes between the (1 × 1)-Bi and (1 × 2)-Bi phases are more subtle. The cation-related S_4-state, and the anion-related S_5- and S_6-states, shift to lower binding energies by 0.12 eV and 0.2 eV, respectively. These small energy shifts are probably caused by distortion of the Bi chains and differences in bonding to the substrate, upon formation of the reconstructed Bi layer. Similar shifts and increasing of spectral density at the Fermi energy have also been observed for the (1 × 2)-Bi/GaSb(110) system [14, 15]. According to the GIXD results [12] (figure 6), the (1 × 2) reconstruction involves deeply both substrate and overlayer atoms, determining strong variations of bond lengths and angles relative to the ECLS (1 × 1) geometry. These variations make each overlayer atom of the unit cell strongly inequivalent, probably causing a modification of the $S_{7,8}$-states (related to the Bi dangling bonds), on passing from the (1 × 1) to the (1 × 2) reconstruction, and thus giving rise to the S'- and S''-states.

The electronic properties of the (1 × 2)-Bi phase have also been studied by means of HREELS. The HREEL spectra of the clean InAs and (1 × 2)-Bi phase are shown in figure 10,

in the energy range of the electronic transitions across the semiconductor band-gap. In the (1×2)-Bi phase the substrate band-gap is filled, confirming the metallic character of the system. The spectrum shows two further features, labelled as A and B in figure 10, with maxima located at 440 and 870 meV loss energy, respectively. They correspond to maxima in the joint density of states between filled and empty surface states across the bulk gap. Taking into account the energy position of A and B and the binding energies of the highest occupied S'-, S''-states, we infer a maximum in the density of empty electronic states at approximately 0.3 eV higher energy than the InAs conduction band minimum (considering the RT band-gap value of 0.36 eV).

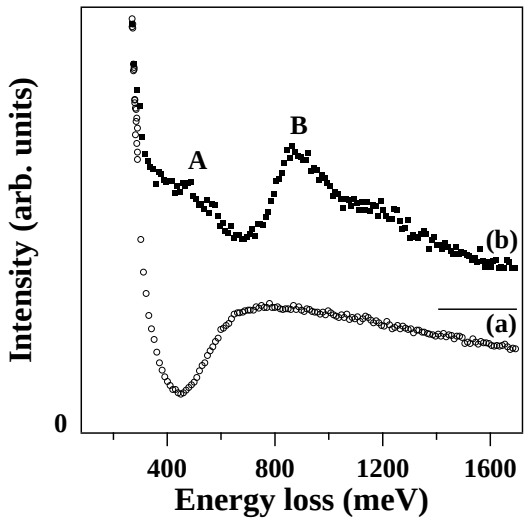

Figure 10. HREEL spectra in the low-energy electronic excitation region, for the clean InAs(110) surface (a) and the (1×2)-Bi phase (b). Curves are vertically shifted for clarity. Primary beam energy E_p: 21.4 eV; angle of incidence and collection: 60°.

The problem of band-bending evolution upon the formation of a metal/III–V(110) semiconductor interface has been widely addressed. In particular, the deposition of different adsorbates on the narrow-gap InAs(110) surface has often been found to lead to an accumulation layer [21]. Measurements on the Bi/InAs(110) interface are, as far as we know, still lacking. We therefore studied the band-bending evolution upon Bi adsorption, analysing both the core-level and the HREELS plasmon–phonon mode energy shifts. While the former gives direct information on the band-bending potential, the latter is related to modification of the free-carrier density in the interfacial region [22–24]. The HREEL spectra in the plasmon–phonon mode energy-loss region are shown in figure 11(a) for the Bi/InAs(110) system, at increasing Bi coverage up to 2 ML. Upon Bi adsorption, the high-energy plasmon–phonon mode (plasmon loss) clearly shifts to higher energies, with a maximum around 0.2 ML, then decreases to an intermediate value at 1 ML coverage. This behaviour is displayed in figure 11(b), along with the shift of the In 4d core-level peak (bulk component) as determined by the best-fit procedure. The two trends are in very good agreement, confirming the comparability of the two measurements. In the first adsorption stages, Bi induces a small accumulation layer that lowers the surface bands by 35 meV at 0.2 ML coverage. With increasing coverage the band bending decreases, leaving a tiny accumulation layer of 10 meV at 1 ML. The (1×2)-Bi phase is also slightly accumulated by 38 meV. The recovered clean surface

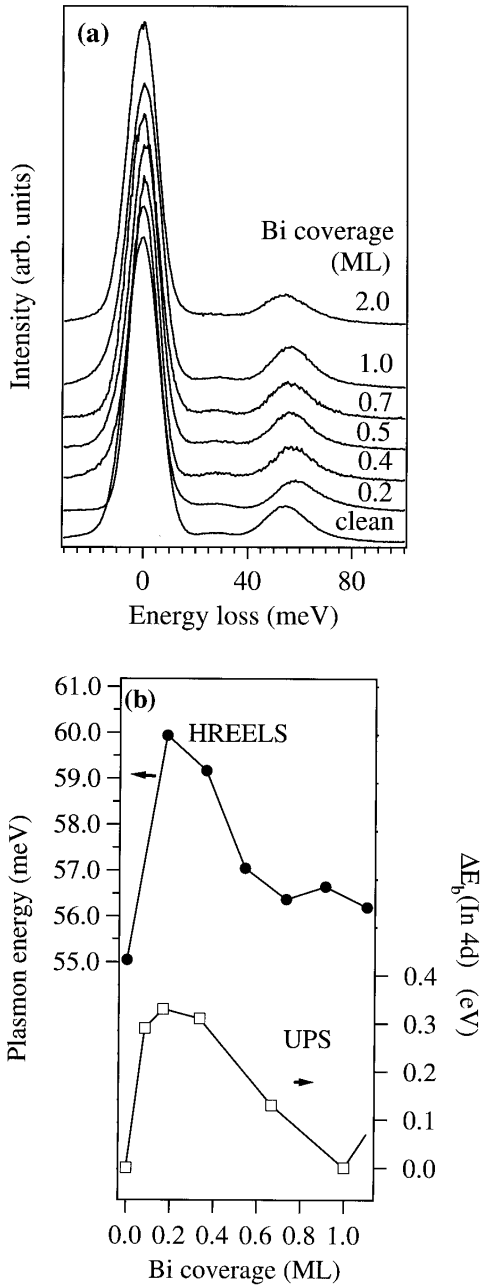

Figure 11. (a) HREEL spectra in the plasmon–phonon energy region of the Bi/InAs(110) system, as a function of Bi coverage. Curves are vertically shifted for convenience. Primary beam energy: 21.4 eV; incidence and collecting angle: 60°. The plasmon energy loss at the clean surface is 55 meV. (b) Plasmon energy (filled circles, left scale) and binding energy shift ΔE_b of the In 4d core level (empty squares, right scale), as functions of Bi coverage.

presents an 80 meV band bending relative to the freshly cleaved InAs(110) surface, this effect being induced by a small density of defects (as deduced from the valence band shape).

Therefore, whatever surface modification is induced (adatom adsorption, defect formation, etc) an accumulation layer is produced on InAs(110). This probably relies on the electronic band structure of InAs, characterized by a narrow gap strongly localized in the k-space around the Γ point.

4. Conclusions

The Bi/InAs(110) system presents two distinct ordered phases characterized by different (1×1) and (1×2) geometrical structures, which are valuable models for 2D ordered systems. Furthermore, they provide the opportunity to study the strong interplay between structural, electronic, and dielectric properties in ordered systems. In order to gain a deeper insight into this issue, we followed the formation of the (1×1) and the (1×2) Bi phases, and studied their properties by means of Auger spectroscopy, HRUPS, HREELS, and LEED. While the (1×1)-Bi phase is semiconducting, the (1×2)-Bi system displays a clear finite spectral density of states at the Fermi energy. According to *ab initio* pseudopotential calculations [4], the geometric structure of the (1×1)-Bi phase is the so-called ECLS, common to most of the other (1×1)V/III–V(110) systems. For the (1×2)-Bi phase, GIXD measurements [12] determine a structure characterized by a strong restructuring of both the adlayer and the substrate, with a substrate missing-row chain reconstruction. Our UPS results are interpreted within this model, in which all substrate dangling bonds are saturated. It is worth noticing that the saturation of the surface dangling bonds can make this major reconstruction energetically more favourable in comparison to a simple Bi missing-row reconstruction. The different geometric structures deeply affect the electronic and dielectric properties of the two phases: due to the strong overlayer chain distortion, the Bi-induced electronic states of the (1×2) phase are shifted in energy relative to the corresponding states of the (1×1)-Bi phase, and thus determine its metallic character. The differences in Bi bonding to the substrate could also be important for determination of the dielectric character of the two structures. A complete understanding of the (1×2) phase electronic states obviously requires an *ad hoc* calculation.

Acknowledgments

This work was financed under a LOTUS Advanced Research Project (INFM), by MURST under 40%-cofin and 60% contracts, and by Consiglio Nazionale delle Ricerche (CNR).

References

[1] Schmidt W G, Bechstedt F and Srivastava G P 1996 *Surf. Sci. Rep.* **25** 141 and references therein
[2] Skeath P, Lindau I, Su C Y and Spicer W E 1981 *J. Vac. Sci. Technol.* **19** 556
[3] Mailhiot C, Duke C B and Chadi D J 1985 *Phys. Rev.* B **31** 2213
[4] Umerski A and Srivastava G P 1995 *Phys. Rev.* B **51** 2334
[5] Ludeke R, Taleb-Ibrahimi A, Feenstra R M and McLean A B 1989 *J. Vac. Sci. Technol.* B **7** 936
[6] Joyce J J, Anderson J, Nelson M M and Lapeyre G J 1989 *Phys. Rev.* B **40** 10 412
[7] Compañó R, del Pennino U and Mariani C 1992 *Phys. Rev. Lett.* **68** 986
[8] Mattern-Klosson M, Strümpler R and Lüth H 1986 *Phys. Rev.* B **33** 2559
[9] Annovi G, Betti M G, del Pennino U and Mariani C 1990 *Phys. Rev.* B **41** 11 978
[10] Ford W K, Guo T, Lantz S L, Wan K, Chang S-L, Duke C B and Lessor D L 1990 *J. Vac. Sci. Technol.* B **8** 940
[11] van Gemmeren T, Lottermoser L, Falkenberg G, Seehofer L, Johnson R L, Gavioli L, Mariani C, Feidenhans'l R, Landemark E, Smilgies D and Nielsen M 1998 *Phys. Rev.* B **57** 3749
[12] Betti M G, Berselli D, Mariani C, Jedrecy N, Sauvage M, Garreau Y and Pinchaux R 1999 *Phys. Rev.* B **59** 15 760
[13] Berselli D, Betti M G, Gavioli L and Mariani C 1995 *Surf. Sci.* **331** 496

[14] Gavioli L, Betti M G, Casarini P and Mariani C 1994 *Phys. Rev.* B **49** 2911
[15] Gavioli L, Betti M G, Casarini P and Mariani C 1995 *Phys. Rev.* B **51** 16 822
[16] Betti M G, Corradini V, del Pennino U, De Renzi V, Fantini P and Mariani C 1998 *Phys. Rev.* B **58** R4231
[17] McIlroy D N, Heskett D, Swanston D M, McLean A B, Ludeke R, Munekata H, Prietsch M and DiNardo N J 1993 *Phys. Rev.* B **47** 3751
[18] McLean A B 1990 *J. Phys.: Condens. Matter* **2** 1027
[19] Joyce J J, Nelson M M, Tang Ming, Meng Y, Anderson J and Lapeyre G J 1990 *J. Vac. Sci. Technol.* A **8** 3542
[20] Spindt C J, Cao R, Miyano K E, Lindau I, Spicer W E and Pao Y-C 1990 *J. Vac. Sci. Technol.* B **4** 974
[21] Aristov V Yu, Grehk M, Zhilin V M, Taleb-Ibrahimi A, Indlekofer G, Hurych Z, Le Lay G and Soukiassian P 1996 *Appl. Surf. Sci.* **104/105** 73 and references therein
[22] Matz R and Lüth H 1981 *Phys. Rev. Lett.* **46** 500
[23] Many A, Wagner I, Rosenthal A, Gersten I J and Goldstein Y 1981 *Phys. Rev. Lett.* **46** 1648
[24] Chen Y, Hermanson C and Lapeyre G J 1989 *Phys. Rev.* B **39** 12 682